A synthetic spring-neap tidal cycle for long-term morphological modelling

R.A. Schrijvershof[1,2], D.S. van Maren[2,3,4], P.J.J.F Torfs[1], A.J.F. Hoitink[1]

[1]Wageningen University & Research, Environmental Sciences Group, Wageningen, The Netherlands
[2]Deltares, Delft, The Netherlands
[3]Delft University of Technology, Faculty of Civil Engineering and Geosciences, The Netherlands
[4]State Key Lab of Estuarine and Coastal Research, East China Normal University, Shanghai, China

Key Points:

- A new method to devise boundary conditions for long-term morphological simulations is introduced
- Estuarine morphodynamic simulations improve when spring-neap tidal variations are accounted for
- The new tidal input reduction method allows to better represent tidal dynamics, bed shear stresses, and residual sand transport

Corresponding author: R.A. Schrijvershof, reinier.schrijvershof@wur.nl

Abstract

Existing tidal input reduction approaches applied in accelerated morphodynamic simulations aim to capture the dominant tidal forces in a single or double representative tidal cycle, often referred to as a "morphological tide". These heavily simplified tidal signals fail to represent the tidal extremes, and hence poorly represent the intertidal areas that exert a major impact on the development of tidal asymmetry. Here, a generic method is developed to construct a synthetic spring-neap tidal cycle that (1) represents the original signal; (2) is exactly periodic; and (3) is constructed directly from full-complexity boundary information. The starting point is a fortnightly modulation of the semi-diurnal tide to represent spring-neap variation, while conserving periodicity. Diurnal tides and higher harmonics of the semi-diurnal tide are included to represent the asymmetry of the tide. The amplitudes and phases are then adjusted to give a best fit to histograms of water levels and water level gradients. A depth-averaged model of the Ems estuary (The Netherlands) demonstrates the effects of alternative tidal input reduction techniques. Adopting the new approach, the shape of the tidal wave is well-represented over the entire length of the estuary, leading to an improved representation of extreme tidal conditions. In particular, representing intertidal dynamics benefits from the new approach, which is reflected by a more accurate simulation of residual sand transport fluxes throughout the estuary. Morphological simulations forced with the synthetic signal approach non-schematised tidal dynamics, which improves the overall predictive capacity of morphodynamic models.

Plain Language Summary

The time-scales of erosion and deposition processes in estuaries and tidal basins is several orders of magnitude larger than the time scales of the changing flows (years versus hours, respectively). To bridge this gap, an acceleration factor is applied to estuarine and coastal models that simulate the long-term bed level developments. Tidal information used to force these accelerated models at the seaward boundary requires an exactly repetitive signal to avoid inconsistencies in the up-scaling approach. A tidal input reduction technique is required to cope with the fact that tides are constantly changing. In this paper, a tidal input reduction method is developed that yields a synthetic, periodic tidal signal representing the variation of amplitudes and asymmetries present in a multiyear tidal signal. The results from a numerical model forced with the synthetic tidal signal shows that intertidal dynamics and residual sand transports improve with respect to existing, more limited, approaches for tidal input reduction. The new tidal input reduction method improves the exchange between channels and intertidal areas in long-term estuarine and coastal models, allowing for a more realistic assessment of erosion and deposition in these areas.

1 Introduction

The long-term or multi-decadal evolution of estuaries and tidal basins is largely controlled by the interaction between the hydrodynamic forcing and the sediment bed (Dam et al., 2016). Such a clear dependence of estuarine morphodynamics on hydrodynamic controls allows for a quantitative investigation on the evolution of tidal basins using numerical models. Although numerical bed evolution models are often developed to predict the direct morphological response to engineering measures, they appear to be more realistic when the time scales related to the investigated changes (T_c) and the time-scale at which the model attains dynamic equilibrium (T_e) are longer (Hoitink et al., 2020). Therefore, process-based modelling has become an increasingly popular tool to investigate not only decadal but also centennial and even millennial morphological evolution of estuarine and tidal environments (e.g.; Dastgheib et al., 2008; van der Wegen & Roelvink, 2012; Nnafie et al., 2018).

Long-term morphological modelling requires appropriate up-scaling of the effects of hydrodynamic processes that typically fluctuate within hours or days to the time periods relevant for morphological changes. Various techniques exist to bridge this gap, ranging from postponed morphological updating, based on gradients in the tide-averaged residual transport, to constructing simplified sediment balances that express bottom change in terms of sediment transport gradients depending only on the local water depth (Latteux, 1995; de Vriend et al., 1993; Roelvink, 2006; Roelvink & Reniers, 2011). The most commonly used morphological updating technique is the fully coupled approach, referred to as the online approach (Roelvink, 2006), where the bed level is updated every hydrodynamic time step. Such continuous updating includes short-term interactions between flow, sediment transport, and morphology while maintaining a relatively stable bed evolution, also in intertidal areas which are inundated during high water only. For reasons of computation efficiency, long-term morphological evolution requires the additional use of a so-called morphological time scale factor (or MorFac, MF), essentially a multiplication factor for the depth change rate (Roelvink & Reniers, 2011). The MF approach produces relatively consistent bed evolution patterns for values up to $O(1000)$, as long as no irreversible changes develop within a phase of the tidal cycle (Van Der Wegen & Roelvink, 2008).

Long-term simulations using the MF approach require schematised boundary conditions representing a repetitive pattern of conditions that include the dominant forcing conditions, but exclude large fluctuations that can result in unrealistic bed-evolution. The goal of input reduction is therefore to derive a limited subset of representative conditions that result in the same residual transport and associated morphological change patterns compared to a simulation forced with the full complexity time-series over the period of interest (i.e. a 'brute-force' simulation).

Existing methods for tidal input reduction aim at capturing the dominant tidal forces in a single (e.g. Dastgheib et al., 2008) or double representative tidal cycle (Latteux, 1995; Lesser, 2009). Simplifying the tidal signal to these very limited conditions seems justified, as many authors have shown to simulate representative residual transport fluxes and the resulting morphological changes of the tidal channels (van der Wegen & Roelvink, 2012; Van Der Wegen et al., 2011; Dissanayake et al., 2009; Dastgheib et al., 2008). However, heavily simplified tidal signals fail to represent the tidal extremes. They poorly represent intertidal areas, which exert a major impact on the development of tidal asymmetry (Friedrichs & Aubrey, 1988). Although the tide-averaged transport of non-cohesive sediments in the main estuarine channels is captured well with solely a semi-diurnal tide and relevant overtides (Van de Kreeke & Robaczewska, 1993), the long-term morphological development of tidal basins is driven by tidal asymmetries resulting from the combination of multiple tidal constituents (Guo et al., 2016). Preserving asymmetries present in the original tidal signal in the tidal input reduction method seems therefore a key requirement. Despite their common use for long-term morphological modelling, the effectivity of tidal input reduction methods has rarely been systematically investigated.

The aim of this paper is twofold. First, a tidal input reduction technique is introduced that yields a synthetic tidal signal representing the tidal extremes as well as tidal asymmetry, which can be used for long-term morphological simulations. Second, the impacts of both existing as well as the new tidal input reduction approaches are systematically investigated. For this latter purpose we develop and apply a morphostatic (no bed level updating) model of the Ems estuary (The Netherlands).

The structure of the remainder of this paper is as follows. We first review existing tidal input reduction techniques and explain the new methodology (Section 2). We then develop a numerical model of a real-world estuary (The Ems estuary, Section 3) and apply this to examine the effect of various types of tidal input reduction (Section 4). The implications of simplifying tidal signals is discussed in Section 5, and conclusions are drawn in Section 6.

2 Tidal input reduction

2.1 The morphological tide

The goal of tidal input reduction is to represent a signal of tidal fluctuations, resulting from the numerous astronomical and non-astronomical tidal frequencies, with a simplified tide. The simplified tidal signal is supposed to represent the original signal in a sense that it produces the same residual transport or morphological change patterns for a defined period and region of interest, and provide a signal with a cyclic period to construct a repetitive pattern of forcing conditions. Such a simplified tide is often referred to as the "morphological tide" (Latteux, 1995).

The most common method to derive a morphological tide can be summarised as follows (Roelvink & Reniers, 2011). The morphological development over a sufficiently long time period (e.g.: a spring-neap cycle) is executed with both full hydrodynamic forcing and with several accelerated simulations, each forced with a single tidal cycle, selected from the time-series. The patterns of residual transport or bed level adaptations resulting from reduced input and from the full forcing are subsequently compared based on a correlation coefficient and the slope of the regression. The simplified tidal cycle that best resembles the full forcing simulation is then considered most representative.

Lesser (2009) demonstrated that such a simplified tide fails to correctly represent residual transport in some cases, because it neglects the asymmetry resulting from interaction between the main semi-diurnal constituent (M_2) and the main diurnal constituents (O_1 and K_1). Hoitink et al. (2003) demonstrated that in diurnal, or mixed mainly diurnal regimes a residual transport can develop resulting from the tidal asymmetry that arises from these primary constituents because they have angular frequencies that consist of sums and differences of two of the basic astronomical frequencies (see Pugh, 1987), leading to substantial residual transport and morphological changes (Van Maren et al., 2004; Van Maren & Gerritsen, 2012). In these regimes, the residual transport that arises from the triad interaction of K_1, O_1 and M_2 can be more important than the residual transport caused by the non-linear interaction of the main semi-diurnal component (M_2) with its first overtide (M_4) (Song et al., 2011), often considered to be the dominant mechanism for shallow water tides (e.g., Friedrichs & Aubrey, 1988; Van de Kreeke & Robaczewska, 1993). Lesser (2009) therefore included this triad interaction by defining an artificial constituent C_1 with half the frequency of the M_2 tidal constituent. The resulting *double tide* consists of C_1, M_2 and its overtides, and an additional scaling factor on M_2 and/or C_1 to account for the presence of a residual flow.

A literature review of 25 publications (including the publications cited in this article) that apply accelerated (2Dh or 3D) morphological models in tide-dominated settings reveals that tidal forcing is often reduced to the M_2 tidal constituent (11 publications), M_2 and its overtides (3 publications), or the morphological *double tide* (3 publications). These studies aim at capturing the dominant tidal forces in a single or double representative tidal cycle. However, the simulated long-term morphodynamic development of estuarine environments is determined by the combined effects of asymmetries resulting from the interaction of multiple tidal constituents and river-tide interaction. Particularly, the omission of the S_2 constituent reduces the river-tide interaction and tidal asymmetry (Guo et al., 2016). In 7 publications the authors chose to apply no tidal input reduction and to accept the errors introduced in the sediment balance due to the absence of a cyclic tide. These studies, however, focused on decadal time-scales with small acceleration factors. For long-term simulations, a simplified cyclic tide representing all significant tidal constituents (and therefore their interactions) would be an important advance over earlier simplified tides (Guo et al., 2016).

2.2 A synthetic representative signal

We aim to develop a generic method to construct a synthetic representative tidal signal that incorporates tidal extremes in a spring-neap cycle, while remaining periodic. The target synthetic spring-neap cycle: (1) sufficiently represents the original signal to preserve asymmetries; (2) is periodic, to ensure consistency in the start and end of consecutive cycles and to control the relative phasing with other types of forcings (e.g.: wind, waves, discharge); and (3) is derived in a deterministic way, to avoid the empirical procedure required for the *morphological tide*, which introduces a dependency on the parameters and the locations chosen for the analysis.

The construction of the synthetic signal starts with a fortnightly modulation of the amplitude of the semi-diurnal tide to represent spring-neap variations. A fortnight represents the real-world amplitude and phase variation much better than a single or double tide. Higher harmonics of the semi-diurnal tide are included to represent the asymmetry of the tide. Diurnal tides are included, following the method of Lesser (2009) to account for the O_1-K_1-M_2 interaction while maintaining periodicity of the signal. The synthetic signal is given by:

$$\begin{aligned} \zeta(t) = \\ \left(\overline{A_{D_2}} + A_{D_{sn}} \cos(\omega_{sn} t)\right) \cos(\omega_{D_2} t - \phi_{D_2}) \\ + \overline{A_{D_4}} \cos(\omega_{D_4} t - \phi_{D_4}) \\ + \overline{A_{D_6}} \cos(\omega_{D_6} t - \phi_{D_6}) \\ + \overline{A_{D_8}} \cos(\omega_{D_8} t - \phi_{D_8}) \\ + \overline{A_{C_1}} \cos(\omega_{C_1} t - \phi_{C_1}) \end{aligned} \tag{1}$$

where $A_{D,n}$ is the amplitude, $\omega_{D,n}$ the angular frequency, and $\phi_{D,n}$ the phase of the n^{th} tidal constituent. The angular frequency ω_{D_2} is taken equal to ω_{M_2}, and all other angular frequencies are an integer product or one over an integer product of this primary forcing frequency. The diurnal C_1 constituent has an amplitude of $\sqrt{2A_{O_1}A_{K_1}}$ and the phase average of ϕ_{O_1} and ϕ_{K_1}. The overbar denotes time-averaging and t is time. The amplitude of D_{sn} modulates $\overline{A_{D_2}}$ and is equal to the amplitude of the second largest peak in the semi-diurnal frequency band, which corresponds to S_2 or N_2. The length of the "morphological spring-neap cycle" we introduce is given by the closest even number (denoted by i) of D_2 cycles that fit into the length of the spring-neap period induced by M_2-S_2 interaction; exactly 28 semi-diurnal cycles. The angular frequency of the fortnightly modulation is then given by

$$\omega_{sn} = \frac{2\pi}{28 T_{D_2}} \tag{2}$$

where T_{D_2} is the period of the D_2 constituent.

The step-wise construction of the morphological spring-neap cycle is illustrated in Figure 1, using a 19-year record of water level observations collected in the Dutch North Sea (station Wierumergronden). The synthetic signal is compared with the full tidal signal using histograms of the free surface elevation (ζ) and the surface level gradient ($d\zeta/dt$). Those histograms capture different types of asymmetry present in a tidal signal (Guo et al., 2019). The histogram of ζ indicates asymmetry in tidal peaks, i.e. tidal peak asymmetry, and the histogram of $d\zeta/dt$ indicates asymmetry in the duration of the rising and falling limbs of the surface elevation time-series, referred to as tidal duration asymmetry. This approach based on histograms concisely characterises tidal asymmetry resulting from all constituents, in contrast to the harmonic method that characterises the asymmetry resulting from two or more interacting constituents. The histograms in Figure 1 illustrate how the addition of the individual terms of Equation 1 provide a signal that progressively better represents the nearly complete tidal signal (reconstructed with 68 significant constituents resolved through harmonic analysis, see Pawlowicz et al. (2002)).

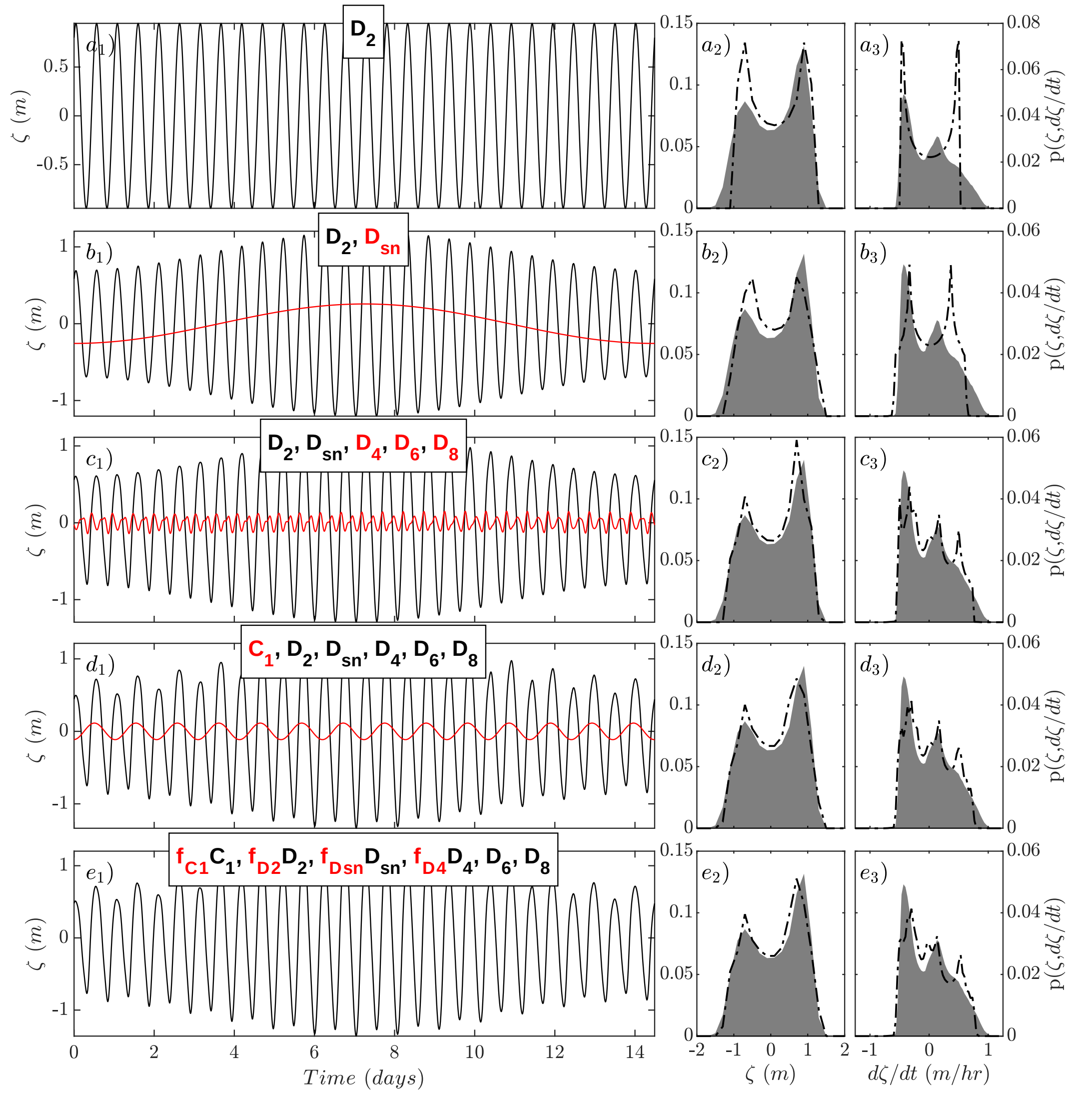

Figure 1. Step-wise construction of the synthetic spring-neap cycle, adding constituents in panel a-d, and scaling in panel e. For each step the resulting time-series (subscripted by 1) are shown in black and the added tidal constituent in red. The panels subscripted by 2 and 3 show the histograms of the synthetic signal (dashed line) and the full tidal signal (gray patch) for ζ and $d\zeta/dt$, respectively.

Applying basic trigonometry, the synthetic signal is rewritten as a linear combination of sines and cosines with zero phases, which facilitates the optimisation. This equation is fitted to the full astronomical tidal signal using scale factors to the amplitudes of the sines and cosines of D_2, D_{sn}, C_1, and D_4 (higher harmonics of D_2 are not scaled because of time efficiency in the algorithm). A combined Root-Mean-Squared-Error (RMSE) for the histogram of ζ and $d\zeta/dt$ is computed for each individual scaling factor. The error values are stored in a matrix to optimise the combination of scaling factors for the amplitudes of each tidal constituent.

The degree in which the resulting synthetic spring-neap cycle and other simplified tidal signals represent the full tidal signal and its asymmetries is visualised in Figure 2.

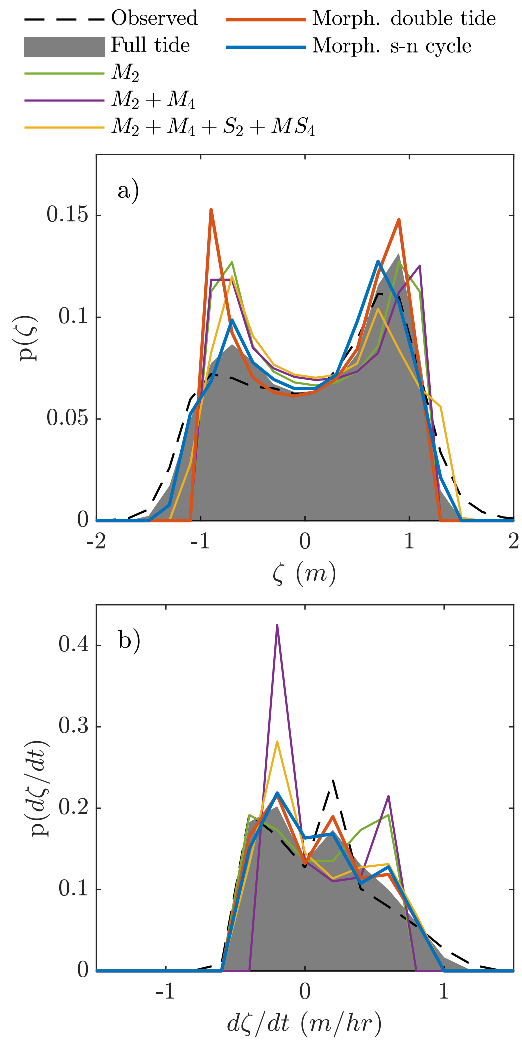

Figure 2. Histograms of ζ (a) and $d\zeta/dt$ (b) for the observed signal (dashed line), a tidal prediction including 68 resolvable tidal constituents (gray patch), and the simplified tidal signals (coloured) generally used for long-term morphological modelling. Histograms are constructed using a bin width of 0.2 m and $\frac{1}{6}$ m/hr for the the histogram of ζ and $d\zeta/dt$, respectively.

Representing the full tide with a single M_2 constituent clearly oversimplifies the signal as this M_2 tide is completely symmetric. Although this is slightly improved by adding an M_4 constituent, tidal extremes are not yet captured. These extremes are better represented when spring-neap variations (M_2+M_4+S_2+MS_4) are included, but the asymmetry of ζ is reversed. The morphological *double tide* represents the asymmetry of $d\zeta/dt$ well, but does not capture the extremes and asymmetry of ζ. The synthetic spring-neap cycle better approximates the extremes and asymmetries in the full tidal signal than the other simplified tides do. The synthetic signal does include, however, a third peak in the histogram of $d\zeta/dt$, which is not present in the full tide. Apparently, this peak is suppressed by tidal constituents other than included in the simplified tide.

3 Numerical model

3.1 Model set-up

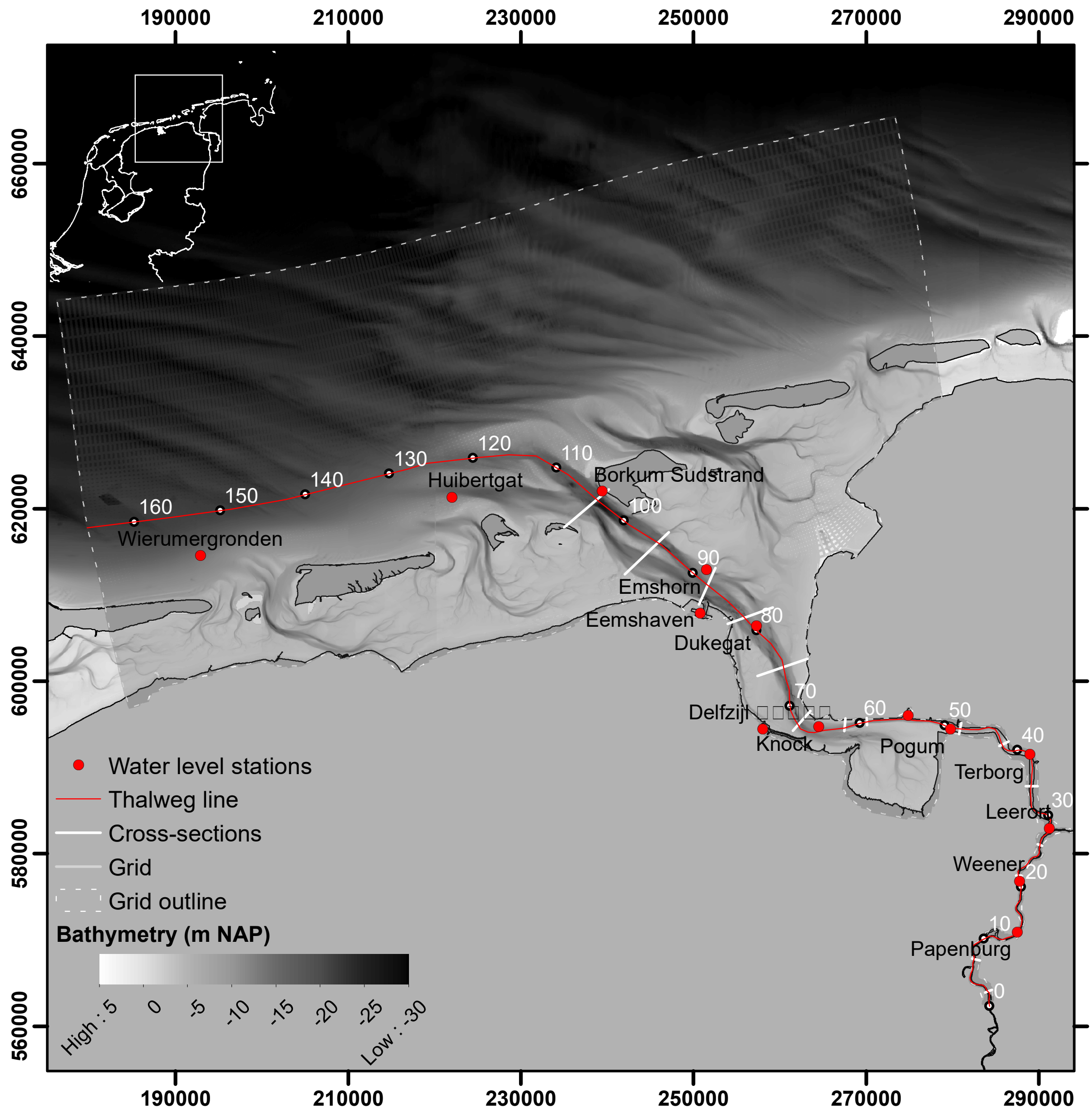

Figure 3. The Ems estuary and numerical model domain (gray lines), with the locations of water level observations (red dots) and a line that follows the main route of tidal propagation (red line) from the western boundary of the model through the thalweg of the estuary and river, with estuary kilometres defined with respect to the point of maximal tidal intrusion at the weir.

A numerical model is developed to quantify how various tidal reduction techniques influence the spatial variation of hydrodynamics and sediment transport. The model is set-up to represent a real-world estuary rather than an idealised case, because the complex topography of a realistic environment introduces tidal asymmetries which provide important benchmarks. For this purpose we have selected the Ems estuary, a meso-tidal system on the Dutch-German border that is part of a large coastal lagoon (the Wadden Sea). The tidal prism is predominantly accommodated by a single channel that aligns with the incoming tidal wave propagation direction, as the tidal wave travels from west to east along the North Sea coast. The discharge of the main river draining into the estuary (the Ems river) varies between 30 - 300 m^3/s, and is small compared to the flood tidal prism (10^9 m^3) (De Jonge et al., 2014).

The model is developed in the Delft3D Flexible Mesh model suite (Kernkamp et al., 2011). The numerical domain covers the offshore coastal part in the Wadden Sea, the estuary, and the river up to an up-estuary weir, with a grid cell size ranging from 1 km (offshore) to 30 m (Figure 3). The model is set-up in 2D depth-averaged (2Dh) mode, with corrections for spiral motion (secondary flow) applied to the depth-averaged momentum equations. Water level boundary conditions are derived from a validated hydrodynamic model that covers the Northwest European Shelf (Zijl & Groenenboom, 2019) for the years 2018-2019. Tidal constituents at the boundaries are adjusted according a comparison between modelled and observed amplitudes and phases, derived through harmonic analysis (Pawlowicz et al., 2002) at station Wierumergronden (close to the western boundary of the model - see Figure 3). One larger river (the Ems River) and a number of smaller rivers drain into the estuary. A time-varying observed river discharge is prescribed for model calibration and validation, whereas a constant value (80 m^3/s for the Ems river and less than 10 m^3/s) for the smaller rivers) is prescribed for various scenario simulations. The bathymetry of the model is based on echosounding observations collected in 2014, which are made freely available by the Dutch Directorate-General for Public Works and Water Management.

Sediment transport is computed with the Van Rijn (1993) formula for medium fine sand (180 μm). The model is executed in morphostatic mode (i.e. no bed update) because the feedback loops initiated by morphological adjustments do not allow for an analysis of the direct effects of the boundary schematisation on residual transport. An equilibrium sand concentration is prescribed at the marine model boundaries, but no sand enters the model domain through the fluvial boundaries. There is interaction with the bed, which has an unlimited sand supply potential.

3.2 Hydrodynamic calibration and validation

Water level observations for the years 2018 - 2019 collected throughout the estuary are used to calibrate and validate the model (see Figure 3). The time-series are decomposed into tidal constituent amplitudes and phases using harmonic analysis (Pawlowicz et al., 2002). In the calibration phase, the model simulates the year 2018, using a spatially uniform roughness coefficient, Mannings' n, amounting to 0.017, 0.019, and 0.021 $m^{1/3}$ s^{-1} (Figure 4). Tidal propagation is best represented by a Manning's n value of 0.019 $m^{1/3}$ s^{-1}. Such a bed roughness, however, overestimates dampening of the tide in the Ems river. In reality, the tides amplify as a result of extensive fluid mud deposits in the Ems River, resulting in an apparent bed roughness around 0.10 $m^{1/3}$ s^{-1} (Van Maren et al., 2015). A linear decrease in bed roughness (from 0.019 $m^{1/3}$ s^{-1} at the entrance of the river towards 0.011 $m^{1/3}$ s^{-1} at the upstream end at the weir) is therefore employed, which better represents the tidal dynamics.

The model was validated against water level observations over the first five months of 2019. The modelled amplitudes of the four primary tidal constituents (M_2, S_2, O_1, K_1) and M_4 are typically within 15% of the observed amplitudes (Figure 5a). The errors are larger (up to 28%) for the S_2 and M_4 tidal constituents in the landward part of the Ems river. Modelled phases are typically within 10° of observations, but the modelled phases of O_1 and especially K_1 differ more than 20° in the tidal river part (Figure 5b).

The calibrated model introduced herein serves to evaluate alternative tidal input reduction approaches for morphological modelling. The non-schematised tidal boundary conditions (full tidal, providing a reference condition) and alternative simplified tidal representations (as in Figure 2) are detailed in Table 1. The boundary forcing with the

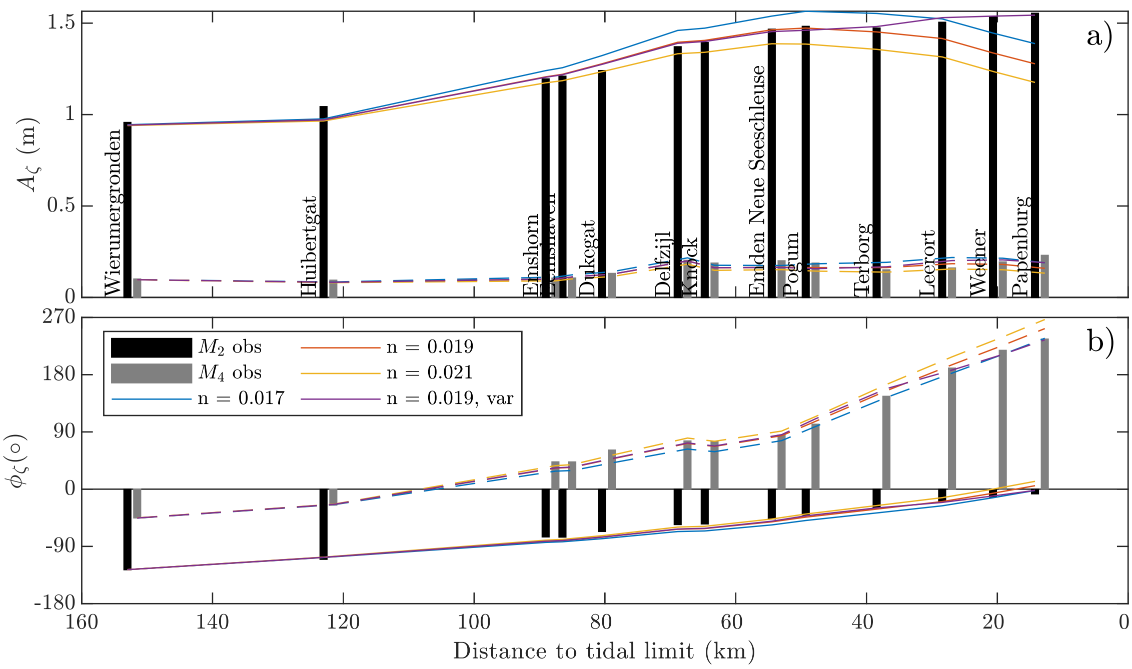

Figure 4. Observed and modelled amplitudes (a) and phases (b) of the M_2 and M_4 tidal constituents, based on the 2018 simulation. Model results (coloured lines) show the effect of different values for a spatially uniform Mannings' n ($m^{1/3}$ s^{-1}) and the best calibrated model with a spatially varying roughness in the Ems river.

morphological *double tide* includes an analytically derived scaling factor for M_2 to account for the presence of a residual flow (cf. Lesser, 2009). The various tidal input reduction scenarios are compared in terms of tidal wave shape, bed shear stress, inundation, and sand transport in the following sections.

Table 1. Duration of the simulations forced with simplified tidal signals and the full tidal simulation that serves as the reference. Simulation names are used in the legends of the figures in the results.

Simulation name	Duration
Full tidal	1 year
M_2	24 hr, 50 min
M_2M_4	24 hr, 50 min
$M_2M_4S_2MS_4$	14.77 days
Morph. double tide	24 hr, 50 min
Morph. spring-neap	14.48 days

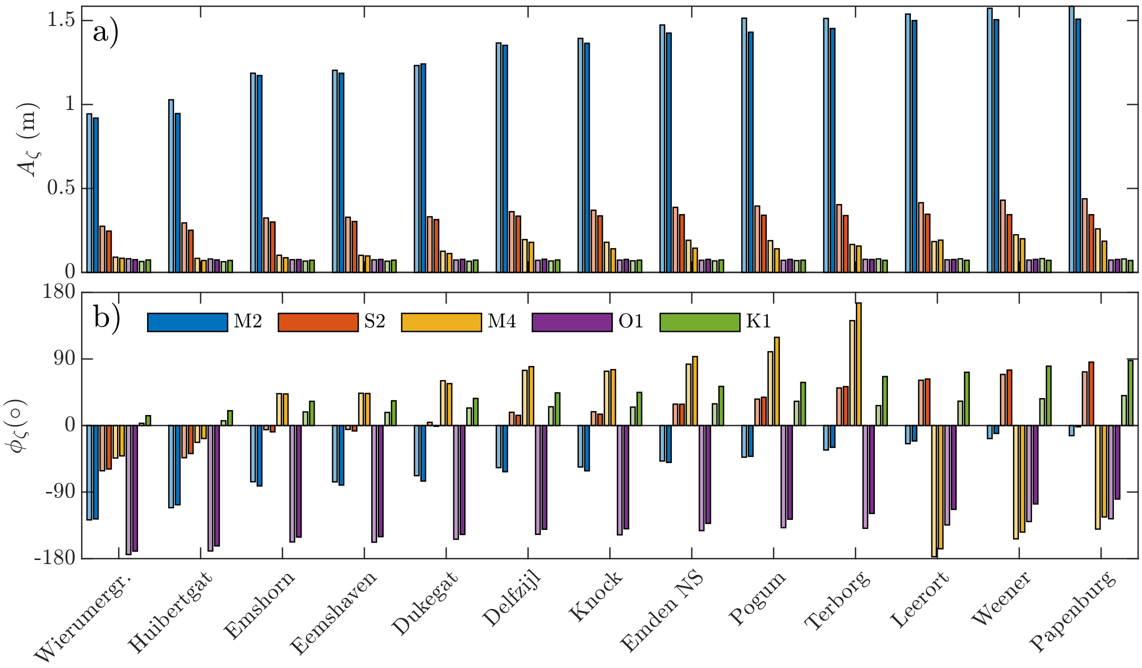

Figure 5. Observed (light coloured) and modelled (dark coloured) tidal constituent amplitudes (a) and phases (b), based on the 2019 simulation.

4 Results

4.1 Tidal wave shape

The representation of tidal wave shape is a primary indicator for the error made in the simulations forced with simplified tidal conditions. Figure 6 quantifies the adequacy of the tidal wave shape representation based on the RMSE between the tidal reduction scenario and the full tidal signal, for histograms of both ζ and $d\zeta/dt$. The figure clearly shows that only using an M_2 boundary forcing leads to the largest error. Including more tidal constituents in the boundary information decreases the error and introducing spring-neap variations ($M_2M_4S_2MS_4$) leads to a markedly better representation of tidal wave shape. The *morphological spring-neap tide* shows the smallest error, both for ζ and for $d\zeta/dt$. The improvement established by introducing spring-neap variations is largest in the coastal and central part of the estuary (km 70 - 160), because error estimates for all tidal reduction techniques converge to the same value in the upper reaches of the estuary. This convergence probably results from an up-estuary morphology that is primarily shaped by the semi-diurnal frequency and its overtides.

4.2 Bed shear stress

Maximum bed shear stress magnitudes along the estuary thalweg (Figure 7a) are most accurately represented when accounting for spring-neap variations, although there still is an underprediction of 30-40%. Including spring-neap variations gives a better representation of tidal wave shape, therefore, asymmetries are better preserved leading to higher maximum tidal velocities. The mean shear stresses in the thalweg (Figure 7b), on the other hand, are represented well by all simplified tides (although they are slightly overpredicted using the morphological *double tide.*). An analysis on the error made in representing bed shear stress magnitudes over the complete model domain, however, in-

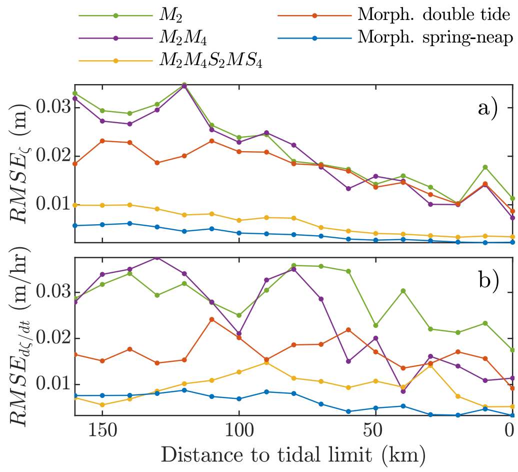

Figure 6. RMSE for the histogram of ζ (a) and $d\zeta/dt$ (b) between the simulations forced with simplified tides and the full tidal simulation, calculated at points in the thalweg along the estuary kilometres defined in Figure 3.

dicates that both maximum (Figure 8a) and mean (Figure 8b) shear stress magnitudes improve by incorporating tidal extremes. A reduction in RMSE is found in the subtidal (channels) and intertidal parts of the model domain. The consistent overprediction of mean bed shear stress magnitudes with the morphological *double tide* in the thalweg (Figure 7b) is reflected by larger RMSE values in the subtidal domain (Figure 8b). Possibly, the overprediction is due to the implementation of a scaling factor for the M_2 tidal amplitude, to account for non-tidal energy in the spectral tidal frequency band.

4.3 Inundation

The intertidal areas, representated by computational cells that experience regular flooding and drying, make up ≈20% of the model domain. In those areas, the duration of inundation strongly controls sediment settling at the bed and therefore, the residence time of water over the tidal flats (Figure 9) is an important property to capture in morphological simulations of tidal environments. Particularly the high littoral zone (Figure 9a, b) is not captured well by the simulations that exclude spring-neap variations, evidenced by too many computational cells that are permanently dry. Sediment cannot settle in the higher intertidal parts when they are not inundated, and tidal flats will not be able to grow to a height that resembles reality. Similarly, in the low littoral zone (Figure 9e, f), the simplified signals without spring-neap variations result in too many computational cells that are permanently inundated such that the lower intertidal zone becomes a subtidal area. Average conditions in the mid-littoral zone are well-represented by all simplified tides.

4.4 Sediment transport

The gross, cross-section integrated sand transport fluxes vary with each tidal cycle in the *full tidal* simulation. The mean of the range in gross transport flood fluxes (Figure 10a) is well-captured by the $M_2M_4S_2MS_4$ tide, the morphological *double tide*, and the morphological *spring-neap* simulations. The M_2 tide, the *morphological double tide*, and the *morphological spring-neap* simulations all reproduce the mean gross ebb transports reasonably well. For the full tidal simulation, the residual transport (Figure 10b) is flood-dominant in the mouth (km 85 - 108), ebb-dominant in the central part (km 45

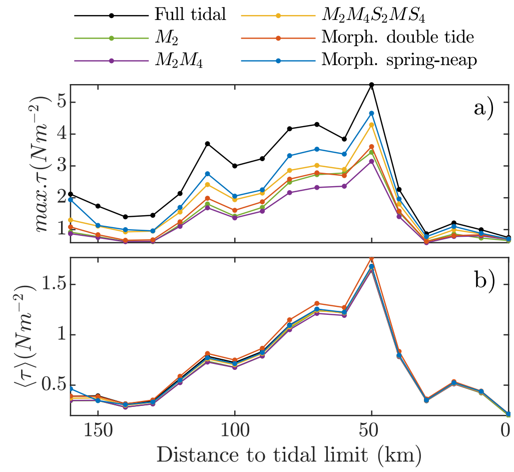

Figure 7. Maximum (a) and mean (b) bed shear stress magnitudes simulated with the full tidal forcing and simplified tides, calculated at points in the thalweg along the estuary kilometres defined in Figure 3.

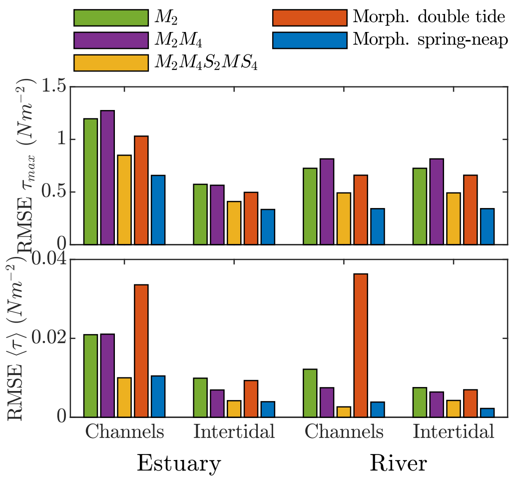

Figure 8. RMSE for the maximum (a) and mean (b) bed shear stress magnitudes between the simulations forced with simplified tides and the full tidal simulation. RMSE values are calculated as mean values for all the computational cells within the specified subregions estuary, river, subtidal channels and intertidal areas.

- 85) of the estuary; and neither flood nor ebb dominant in the tidal river (km 0 - 45). This large-scale behaviour is captured well by each of the alternative simplified tides, except for the M_2 simulation, which prescribes a perfectly symmetric tide at the sea boundaries and therefore leads to an underestimation of the flood directed residual transport (Figure 10a). The morphological *spring-neap* tidal boundary conditions lead to residual transport best representing *full tidal* residual transport (Figure 10b). The M_2M_4 and $M_2M_4S_2MS_4$ tidal boundary condition leads to an underestimation of the magnitude of the residual transport fluxes, and the *morphological double tide* generates slightly more ebb-dominant transport in the entire estuary.

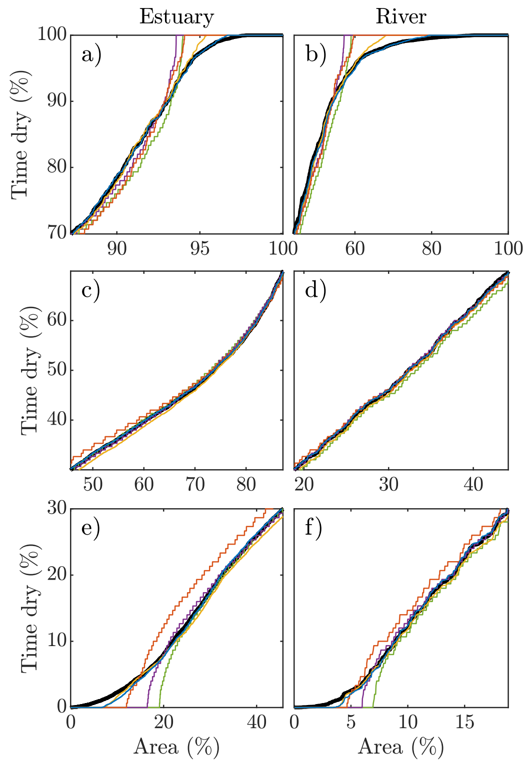

Figure 9. Cumulative distributions of the fraction of time of the total simulation length (in %) that a computational cell is dry (emerged), as a function of the fraction of the total intertidal area in the modelling domain. The distributions are shown for defined subregions; the estuary (a, c, e) and the river (b, d, f), and subdivided in the high (a, b), mid- (c, d), and lower (e, f) littoral zone.

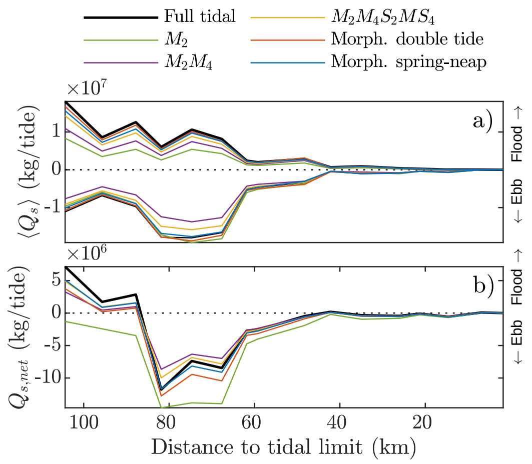

Figure 10. Mean of the total (bed + suspended) load gross transport fluxes (a) and residual transport per tidal cycle (b) in the thalweg (see the cross-sections in Figure 3 for locations).

The morphological evolution is not only driven by the magnitude of gradients in the residual transport flux, but also by the directions. An analysis of the error (RMSE) made in the direction and magnitude of residual transports averaged over all computational cells (Figure 11) reveals that particularly the error in direction is smaller for the simulations that include spring-neap variations. The RMSE for the magnitude of the residual transport shows less scatter, except for the M_2 simulations, which clearly deviates in the channels. In general, including spring-neap variations reduces the error in magnitude and direction of residual transports in the channels and over the intertidal areas.

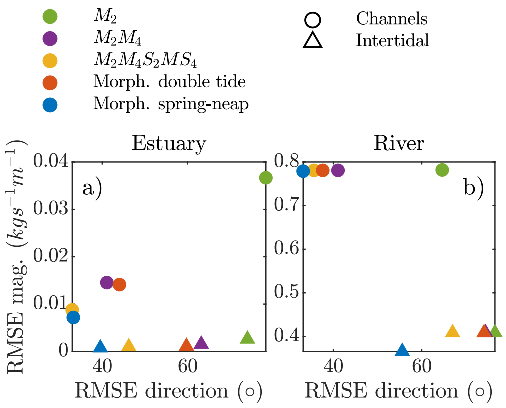

Figure 11. Error (RMSE) in the direction (horizontal axis) and magnitude (vertical axis) of the residual total (bed + suspended) load sand transport in the channels (circles) and on the intertidal areas (triangles).

5 Discussion

A new tidal input reduction method was developed which includes periodic spring-neap variation in a simplified tide. Prescribing this new method as boundary conditions in an estuarine setting improves the representation of tidal wave shape, maximum and mean bed shear stresses magnitudes, inundation times, and residual sand transport patterns, compared to existing tidal input reduction methods to represent the non-schematised tidal dynamics. The strong and weak points of the new methodology and existing tidal input reduction techniques are summarised in Figure 12 using normalised scores, with 0 poorly representing the full tidal signal, and 1 best representing the full signal. The new method scores maximally on 10 out of 12 metrics, with one being the duration of the cycle and the other one being a second-best score for inundation duration. These results therefore motivate to replace traditional approaches for tidal input reduction with the new method.

The main drawback of the synthetic spring-neap cycle, following directly from Figure 12, is the simulation time. The 28 M_2 cycles ($\approx$ 14.48 days) required in the computations is 14 times longer than the time required to simulate a cycle of the morphological *double tide* (Lesser, 2009). In practice, this drawback may be minor, because a shorter representative tidal period (e.g. the M_2 period) is often frequently repeated. The reason for this, is that the bed elevation changes over a single tidal cycle are small compared to inaccuracy, which is then linearly amplified by a comparatively large morphological upscale factor (MF). For this reason, a single morphological tidal cycle is repeated even more often than 28 times, up to multiple hydrodynamic years (e.g. Dastgheib et al., 2008). The longest acceptable hydrodynamic simulation time is then usually combined with the smallest possible MF because large values for the MF can produce unrealistic bed development (Ranasinghe et al., 2011).

Numerical morphological models may also be forced with non-tidal processes, such as a seasonally varying river discharge (e.g. Van Der Wegen et al., 2011) or wave- and wind-driven re-suspension (e.g. Van der Wegen et al., 2017). In these cases, not only the simulation length can be a limiting factor, as the relative phasing of the other forcing factors with the tide explicitly need to be accounted for as well. For instance, persistently combining seasonal river floods or storm events with spring tide or flood conditions leads to unrealistic bed development. Optimizing the relative phasing is much easier with the synthetic spring-neap cycle compared to traditional spring-neap variations, because it is exactly periodic.

According to Van de Kreeke and Robaczewska (1993), a tide-averaged transport for coarse sediment can be achieved by selecting a representative tide consisting of a tide-induced Eulerian mean current (M_0), M_2, and any of its even overtides because they lead to a long-term mean bed-load transport. When diurnal components are important, a net residual transport can arise from the triad interaction of M_2-K_1-O_1 (Hoitink et al., 2003), which can be captured in a periodic double tide trough an artificial diurnal component with half the frequency of M_2 (Lesser, 2009). Spring-neap variations are so far virtually ignored in representative tides (Dastgheib et al., 2008; Roelvink & Reniers, 2011). This paper demonstrates that simplified tides consisting of a single or a double tide (which are most frequently used for long-term morphological modelling) perform well in representing mean bed shear stress and residual sand transports inside the estuarine channels. However, they fail to reproduce maximum bed shear stresses (controlling the timescales of adaptation) and to represent the upper and lower intertidal inundation that steers the development of intertidal flats.

Representing tidal asymmetries is shown to be important to capture the residual sand transports on the intertidal flats as well. This is because the velocity skew (flood versus ebb dominance) over tidal flats is modulated during the spring-neap cycle (Nidzieko & Ralston, 2012). Therefore, if the intertidal parts of the modelling domain are an integral part of the phenomena studied, morphological models can not suffice with a representative tide consisting of a *single* or *double tide*, and improve by including the tidal extremes and asymmetries resulting from the spring-neap modulations.

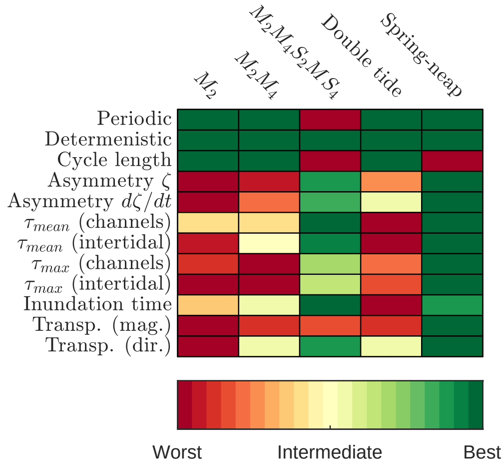

Figure 12. Normalised scores (0-1) for simplified tides to represent non-schematised tidal conditions. Score values are calculated as score $= \frac{x}{\max(1-x/\min(x))}$. The parameters *Periodic* and *Determenistic* are binary, *Cycle length* follows from Table 1, and the scores for the other parameters (evaluated in Section 4) are derived from RMSE values between the simplified tides and the *full tidal* simulation.

6 Conclusions

Spring-neap variations can be included in simplified tidal signals that are applicable as boundary conditions in long-term morphological models. The tidal variation is captured significantly better in a synthetic spring-neap cycle through a fortnightly modulation of the amplitude of the semi-diurnal tide than by a single our double tide. The tidal input reduction method developed in this paper provides a signal that: (1) sufficiently represents the full tidal signal and preserves asymmetries; (2) is strictly periodic; and (3) can be derived directly from the boundary conditions. It does not require a fitting procedure based on modelling results.

Process-based numerical models of tidal environments that include the tidal extremes induced by spring-neap variations represent the shape of the tidal wave through the tidal basin more realistically. Simulations with simplified tidal signals that omit the tidal extremes underestimate maximum bed shear stresses in the channels and simulate a too limited extent of the tidal flats. Although simulations forced with these signals quite reasonably approximate the tidally averaged residual sand transport patterns in the channels, an appropriate representation of the extremes is required to reproduce the patterns both in the channels and on the intertidal areas. The newly developed tidal input reduction method provides a signal that may resolve non-cohesive sediment transport within the estuary more accurately, and improves the simulation of sediment exchange between the channels and tidal flats.

7 Open Research

There is no restriction on the data used in this study. The code for the construction of the synthetic spring-neap tide is written in MATLAB, and available for download at `https://github.com/Rschrijvershof/morphoSpringNeap.git`. The configurations of the numerical model are stored at 4TU.ResearchData (`https://doi.org.10.4121/19845262`).

Acknowledgments

This work was funded by the Netherlands Organisation for Scientific Research (NWO) within Vici project "Deltas out of shape: regime changes of sediment dynamics in tide-influenced deltas" (Grant NWO-TTW 17062) and Deltares Research Funds. The data presented in this paper stem from the Dutch Rijkswaterstaat, the German Wasserstrassen- und Schifffartsamt (WSA) Ems-Nordsee, and the Niedersächsischer Landesbetrieb für Wasserwirtschaft, Küsten- und Naturschutz (NLWKN). The modelling software Delft3D Flexible Mesh was made available by Deltares via the Delft3D Educational Service Package.

References

Dam, G., Van Der Wegen, M., Labeur, R. J., & Roelvink, D. (2016). Modeling centuries of estuarine morphodynamics in the Western Scheldt estuary. *Geophysical Research Letters*, *43*(8), 3839–3847. doi: 10.1002/2015GL066725

Dastgheib, A., Roelvink, J. A., & Wang, Z. B. (2008). Long-term process-based morphological modeling of the Marsdiep Tidal Basin. *Marine Geology*, *256*(1-4), 90–100. Retrieved from `http://dx.doi.org/10.1016/j.margeo.2008.10.003` doi: 10.1016/j.margeo.2008.10.003

De Jonge, V. N., Schuttelaars, H. M., van Beusekom, J. E., Talke, S. A., & de Swart, H. E. (2014). The influence of channel deepening on estuarine turbidity levels anddynamics, as exemplified by the Ems estuary. *Estuarine, Coastal and Shelf Science*, *139*, 46–59. doi: 10.1016/j.ecss.2013.12.030

de Vriend, H. J., Zyserman, J., Nicholson, J., Roelvink, J. A., Péchon, P., & Southgate, H. N. (1993). Medium-term 2DH coastal area modelling. *Coastal Engineering*, *21*(1-3), 193–224. doi: 10.1016/0378-3839(93)90050-I

Dissanayake, D. M., Roelvink, J. A., & van der Wegen, M. (2009). Modelled channel patterns in a schematized tidal inlet. *Coastal Engineering*, *56*(11-12), 1069–1083. Retrieved from `http://dx.doi.org/10.1016/j.coastaleng.2009.08.008` doi: 10.1016/j.coastaleng.2009.08.008

Friedrichs, C., & Aubrey, D. (1988). Nonlinear tidal distortion in shallow well-mixed estuaries. *Estuarine, Coastal and Shelf Science*, *30*(3), 321–322. doi: 10.1016/0272-7714(90)90054-U

Guo, L., Wang, Z. B., Townend, I., & He, Q. (2019). Quantification of Tidal Asymmetry and Its Nonstationary Variations. *Journal of Geophysical Research: Oceans*, *124*(1), 773–787. doi: 10.1029/2018JC014372

Guo, L., Wegen, M. v. d., Wang, Z. B., Roelvink, D., & He, Q. (2016). Exploring the impacts of multiple tidal constituents and varying river flow on long-term, large-scale estuarine morphodynamics by means of a 1-D model. *Journal of Geophysical Research: Earth Surface*, *121*, 1000–1022. doi: doi:10.1002/2016JF003821

Hoitink, A. J., Hoekstra, P., & Van Maren, D. S. (2003). Flow asymmetry associated with astronomical tides: Implications for the residual transport of sediment. *Journal of Geophysical Research: Oceans*, *108*(10), 1–8. doi: 10.1029/2002jc001539

Hoitink, A. J., Nittrouer, J. A., Passalacqua, P., Shaw, J. B., Langendoen, E. J., Huismans, Y., & van Maren, D. S. (2020). Resilience of River Deltas in the

Anthropocene. *Journal of Geophysical Research: Earth Surface*, *125*(3), 1–24. doi: 10.1029/2019JF005201

Kernkamp, H. W. J., Van Dam, A., Stelling, G. S., & De Goede, E. D. (2011). Efficient scheme for the shallow water equations on unstructured grids with application to the Continental Shelf. *Ocean Dynamics*, *61*(8), 1175–1188. doi: 10.1007/s10236-011-0423-6

Latteux, B. (1995). Techniques for long-term morphological simulation under tidal action. *Marine Geology*, *126*(1-4), 129–141. Retrieved from http://dx.doi.org/10.1016/0025-3227(95)00069-B doi: 10.1016/0025-3227(95)00069-B

Lesser, G. (2009). *An Approach to Medium-term Coastal Morphological Modelling*. Retrieved from http://www.narcis.nl/publication/RecordID/oai:tudelft.nl:uuid:62caa573-4fc0-428e-8768-0aa47ab612a9

Nidzieko, N. J., & Ralston, D. K. (2012). Tidal asymmetry and velocity skew over tidal flats and shallow channels within a macrotidal river delta. *Journal of Geophysical Research: Oceans*, *117*(3), 1–17. doi: 10.1029/2011JC007384

Nnafie, A., Van Oyen, T., De Maerschalck, B., van der Vegt, M., & van der Wegen, M. (2018). Estuarine Channel Evolution in Response to Closure of Secondary Basins: An Observational and Morphodynamic Modeling Study of the Western Scheldt Estuary. *Journal of Geophysical Research: Earth Surface*, *123*(1), 167–186. doi: 10.1002/2017JF004364

Pawlowicz, R., Beardsley, B., & Lentz, S. (2002). Classical tidal harmonic analysis including werror estimates in MATLAB using T_TIDE. *Computers and Geosciences*, *28*(8), 929–937. doi: 10.1016/S0098-3004(02)00013-4

Pugh, D. T. (1987). *Tides, surges and mean sea level*. Swindon, UK: John Wiley and Sons Ltd. Retrieved from https://www.osti.gov/biblio/5061261

Ranasinghe, R., Swinkels, C., Luijendijk, A., Roelvink, D., Bosboom, J., Stive, M., & Walstra, D. J. (2011). Morphodynamic upscaling with the MORFAC approach: Dependencies and sensitivities. *Coastal Engineering*, *58*(8), 806–811. Retrieved from http://dx.doi.org/10.1016/j.coastaleng.2011.03.010 doi: 10.1016/j.coastaleng.2011.03.010

Roelvink, D. (2006). Coastal morphodynamic evolution techniques. *Coastal Engineering*, *53*(2-3), 277–287. doi: 10.1016/j.coastaleng.2005.10.015

Roelvink, D., & Reniers, A. (2011). *A Guide to Modeling Coastal Morphology* (Advances i ed.). WORLD SCIENTIFIC. Retrieved from https://www.worldscientific.com/doi/abs/10.1142/7712 doi: 10.1142/7712

Song, D., Wang, X. H., Kiss, A. E., & Bao, X. (2011). The contribution to tidal asymmetry by different combinations of tidal constituents. *Journal of Geophysical Research: Oceans*, *116*(12), 1–12. doi: 10.1029/2011JC007270

Van de Kreeke, J., & Robaczewska, K. (1993). Tide-induced residual transport of coarse sediment; Application to the EMS estuary. *Netherlands Journal of Sea Research*, *31*(3), 209–220. doi: 10.1016/0077-7579(93)90022-K

Van Der Wegen, M., Jaffe, B. E., & Roelvink, J. A. (2011). Process-based, morphodynamic hindcast of decadal deposition patterns in San Pablo Bay, California, 1856-1887. *Journal of Geophysical Research: Earth Surface*, *116*(2), 1–22. doi: 10.1029/2009JF001614

Van Der Wegen, M., & Roelvink, J. A. (2008). Long-term morphodynamic evolution of a tidal embayment using a two-dimensional, process-based model. *Journal of Geophysical Research: Oceans*, *113*(3), 1–23. doi: 10.1029/2006JC003983

van der Wegen, M., & Roelvink, J. A. (2012). Reproduction of estuarine bathymetry by means of a process-based model: Western Scheldt case study, the Netherlands. *Geomorphology*, *179*, 152–167. Retrieved from http://dx.doi.org/10.1016/j.geomorph.2012.08.007 doi: 10.1016/j.geomorph.2012.08.007

Van der Wegen, M., Van der Werf, J., De Vet, L., & Robke, B. (2017). *Hindcasting Westerschelde mouth morphodynamics (1963-2011)* (Tech. Rep.).

Van Maren, D. S., & Gerritsen, H. (2012). Residual flow and tidal asymmetry in the Singapore Strait, with implications for resuspension and residual transport of sediment. *Journal of Geophysical Research: Oceans*, *117*(4), 1–18. doi: 10.1029/2011JC007615

Van Maren, D. S., Hoekstra, P., & Hoitink, A. J. (2004). Tidal flow asymmetry in the diurnal regime: bed-load transport and morphologic changes around the Red River Delta. (January). doi: 10.1007/s10236-003-0085-0

Van Maren, D. S., Winterwerp, J. C., & Vroom, J. (2015). Fine sediment transport into the hyper-turbid lower Ems River: the role of channel deepening and sediment-induced drag reduction. *Ocean Dynamics*, *65*(4), 589–605. doi: 10.1007/s10236-015-0821-2

Van Rijn, L. C. (1993). Principles of sediment transport in rivers, estuaries and coastal seas..

Zijl, F., & Groenenboom, J. (2019). *Development of a sixth generation model for the NW European Shelf (DCSM-FM 100m)* (Tech. Rep.). Delft, The Netherlands: Deltares.